RSC Advances

ROYAL SOCIETY OF CHEMISTRY

www.rsc.org/advances

RSC Advances

ARTICLE

Hydrothermal stability of CeO_2-Al_2O_3 composite, structural study and the oxygen storage capacity

Received 00th January 20xx,
Accepted 00th January 20xx

DOI: 10.1039/x0xx00000x

www.rsc.org/

Guangxi Wei[a], Meiqing Shen [a,b,c], Hang Li[a], Hui Wang[a], Jianqiang Wang[a], Jun Wang[a,*]

A series of CeO_2-Al_2O_3 composites with different Ce content were prepared. The uniformity of CeO_2 dispersion was confirmed by H_2-TPR and HR-TEM. Two aging treatments were conducted, and the CeO_2-Al_2O_3 composites show superior hydrothermal stability. The sintering of CeO_2 and Al_2O_3 are independent with each other based on XRD and HR-TEM results. On the other hand, the dynamic oxygen storage capacity (DOSC) are mostly activated after 750 ˚C 20 h aging, and deactivated after 1050 ˚C 10 h aging. Combining the results of structural and DOSC studies, the interaction between CeO_2 and Al_2O_3 can be devided into two parts, 1) a chemical interaction which negatively impacts the DOSC, and 2) a spatial limitation which benefits the sample stability. The former interaction is eliminated afte 750 ˚C hydrothermal aging, while the later one exist even after 1050 ˚C hydrothermal aging.

Key words: CeO_2-Al_2O_3 composite, hydrothermal stability, oxygen storage capacity, dispersion.

1. Introduction

Exhaust emission control attached more and more public attentions, which brings a great number of studies including the controlling strategy and catalyst design [1]. The catalyst used in emission control always suffers significant deactivation as a result of high temperature and redox oscillations [2], which makes it important to study deactivation process. However, previous studies mostly focus on the evolution of active component [3-4], while the consideration of support oxide is in lack [5]. In this work, the CeO_2-Al_2O_3 composite was prepared, and the intrinsic property and the aging mechanism were studied, as a complementary to the common study about catalyst aging. In TWC, the common used oxygen storage material mainly contains ceria, zirconia and alumina, which is known as the third-generation ceria-zirconia developed by Toyota [6]. The sample system is simplified to only ceria and alumina in our study, for ceria presents obvious oxygen storage capacity (although low than $Ce_{1-x}Zr_xO_2$), which is good enough to understand the interaction between OSC material and alumina, as well as its evolution during hydrothermal aging. And this makes the catalyst design easier and clearer.

The combination of ceria and alumina has been studied long before, which gave the catalyst better low temperature activity and good stability, comparing with the two pure oxides [7-11]. The published synthesize methods can be divided by the mixing strategy, 1) atomic mixing, mixing the Ce and Al source as salt solution (sol method, or co-precipitation) [7], 2) molecular, mixing the CeO_2 crystalline with Al_2O_3 sol [8], and 3) impregnation, impregnating the Ce salt on Al_2O_3 powder [9-11]. The atomic mixing is effective but difficult to control, because of the difference in the dynamics of

[a] *Key Laboratory for Green Chemical Technology of State Education Ministry, School of Chemical Engineering & Technology, Tianjin University, Tianjin 300072, PR China;*
[b] *Collaborative Innovation Centre of Chemical Science and Engineering (Tianjin), Tianjin 300072, PR China;*
[c] State Key Laboratory of Engines, Tianjin University, Tianjin 300072, PR China
† Corresponding author: Jun Wang, Tel.: +86 22 27407002, E-mail: wangjun@tju.edu.cn.
Electronic Supplementary Information (ESI) available: Detail of the kinetic calculation of oxygen storage capacity.

nucleation. On the contrary, impregnation is easily controlled but less effective comparing with the others. Therefore, the molecular mixing strategy was chosen, in order to reach a controllable synthesis and good dispersion of CeO_2. The property of the sample and its evolution in hydrothermal aging were studied.

2. Experimental methods

2.1 Sample preparation

CeO_2 precipitate and Al_2O_3 sol was prepared separately. CeO_2 was prepared by precipitation method. 0.1 M $Ce(NO_3)_3$ solution was dropped into ammonia aqua (analytical grade, KEWEI), when air was bubbled into the reactor to oxidize Ce^{3+}. $NH_3 \cdot H_2O$ used in the reaction was 100 % access than the reaction stoichiometry. After the reaction, the precipitate changes into light yellow by further gas bubbling, and a decay process was conducted with stirring at 90 ˚C for 1 day. After that, CeO_2 precipitate was filtered out, washed and re-dispersed into distilled water. Al_2O_3 sol was prepared by precipitation of 0.1 M $Al(NO_3)_3$ and 3 M $NH_3 \cdot H_2O$. Ammonia was added into $Al(NO_3)_3$ solution dropwisely. At the end of the reaction, the pH of the sol was tuned to 7. This sol was decayed at 60 ˚C for 1 day and at 90 ˚C for another day. Then ceria precipitation and Al_2O_3 sol was mixed together, and PEG-4000 (poly ethylene glycol) was added in a mole-ratio of 0.03 based on the amount of oxide (CeO_2+Al_2O_3). After one hour ultrasonic treatment, the mixture was transferred into a spraying drying device, where the drying process (particle preparation) was finished in several seconds. The obtained sample was calcined at 300 ˚C for 2h and 600 ˚C for 3h. The samples with a Ce mole ratio of 50, 25, 15 and 10 % were prepared and named as CA1, CA2, CA3 and CA4, respectively. The pure ceria and alumina were also prepared with the same method as references, and named as C and A, respectively.

Two hydrothermal aging were conducted, at 750 ˚C 20 h and 1050 ˚C 10 h (both in 10 % H_2O /air) to simulating the aging of diesel and gasoline engine vehicle, respectively. The sample was named as –f (fresh sample), -750 h and -1050h, respectively.

2.2 Characterizations

The mole ratio of CeO_2 in CeO_2-Al_2O_3 composite was determined by X-ray fluorescence (XRF). Surface area measurements were performed on an F-sorb 3400 chemisorption apparatus using BET method. Powder X-ray diffraction (XRD) was measured on an Bruker D8-Focus diffractometer operated at 40 kV and 40 mA with nickel filtered Cu *Kα* radiation (λ=0.15418 nm). The scanning was conducted between 20 and 90˚, with a step speed of 5˚/min. The diffraction peak at 2θ = 28.6˚, according to the CeO_2 (111) face, was used to calculate the average crystalline size using Scherrer equation. SEM (scanning electronic microscopy) images were collected on an S-4800 Scanning Electron Microscope working at 15 KV. Gold deposition was conducted to improve the conductivity of the samples. (HR) TEM images were collected on a Tecnai G2 F20 field emission transmission electron microscope (TEM) working at 200 kV. 0.05 g sample was dispersed into 50 ml alcohol for 1 h, and the dispersion was dropped on an ultra-thin carbon film and dried before the test. H_2-TPR was conducted on a PX200 gas adsorber equipped with a TCD detector. 50 mg sample was packed in a U-type quartz tube reactor. The sample was pre-oxidized with 20 % O_2/N_2 at 500 ˚C for 30 min and cooled down to room temperature. Then it was heated up to 900 ˚C with a rate of 10 ˚C/min, with 5 % H_2/N_2. The total flow rate of reactant gas was 30 ml/min.

Dynamic oxygen storage capacity was tested on a self-designed apparatus. 25 mg sample blended with 40 mg quartz sand was packed in a tubular reactor. The pulse of CO (4% CO/ 1% Ar/ He,

400 ml/min) and O_2 (2 % O2/ 1% Ar/ He, 400 ml/min) was purged into the reactor alternately in a frequency of 0.1 and 0.05 Hz. The gas outlet was analyzed by a Hiden 2.0 mass spectrometer.

3. Results and Discussions

3.1 CeO_2 dispersion in Al_2O_3 framework

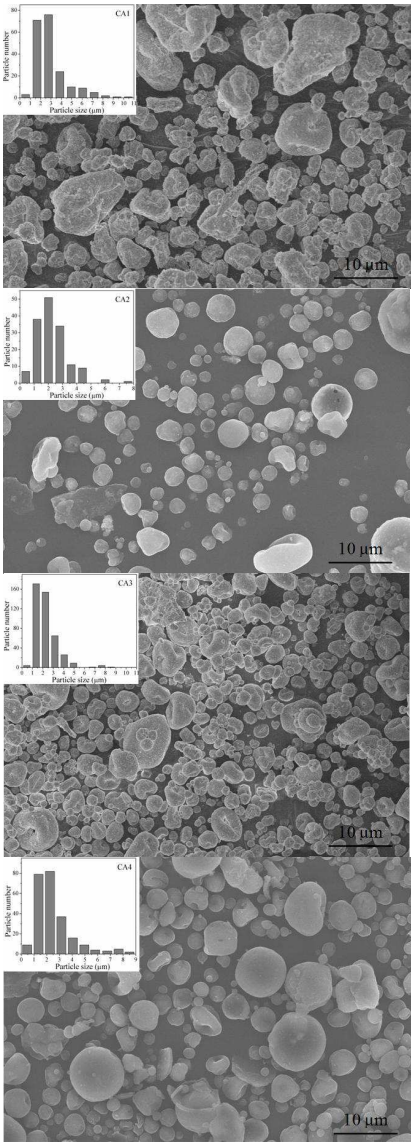

Fig. 1 Sample structure under SEM (Top, CA2-f; bottom, CA4-f)

The molar ratio of $CeO_2/(CeO_2+Al_2O_3)$ is listed in Table 1. On all the samples, the detected Ceria content is slightly larger than the designed value, but within the experimental error. The microstructure of CA particle was observed by SEM, and most of the particles are spheres in size of 1~10 microns. Particle size distribution is displayed in the insect of Fig. 1. Most of the particles are in size of 1~4 μm. No obvious differences is found among different samples, indicates that the physical structure is similar on each sample.

Table 1 BET surface area and CeO_2 crystalline size before and after aging

Sample	Ce ratio	S_{BET} (m^2/g)			D-CeO_2 (nm)		
	(mol %)	F	750h*	1050h*	F	750h*	1050h*
C	100	140	32	3	5.5	18.1	>100
CA1	52	288	157	49	4.5	8.2	33.3
CA2	26	389	224	75	4.6	8.5	29.9
CA3	16	469	224	92	5.1	8.6	29.1
CA4	12	444	225	98	4.7	8.6	24.8
A	0	469	240	42	-	-	-

Since the molar volume of CeO_2 is smaller than the one of Al_2O_3, the CeO_2-Al_2O_3 composites in the presented work can be considered as the CeO_2 crystalline dispersed in Al_2O_3 framework. Therefore, the dispersion is of great importance to the sample property, which was investigated by H_2-TPR. As displayed in Fig. 2, three peaks cantered at 450, 550 and 720 ˚C on CA samples. The reduction temperature is independent to the CeO_2 content, while the peak intensity is roughly proportional to the cerium content (mole ratio). Meanwhile, the pure CeO_2 shows reduction peaks at 390, 507 and 810 ˚C, as surface, subsurface and bulk oxygen, respectively [12]. The deviation of CA composites from pure CeO_2 indicates that the chemical circumstance of CeO_2 in CA composites is different from

the one of pure CeO_2. However, the reduction temperature of each peak is independent to the cerium content (only the intensity is changed). Therefore, the chemical circumstance of CeO_2 is independent of CeO_2 ratio, which infers a uniform dispersion in all the samples.

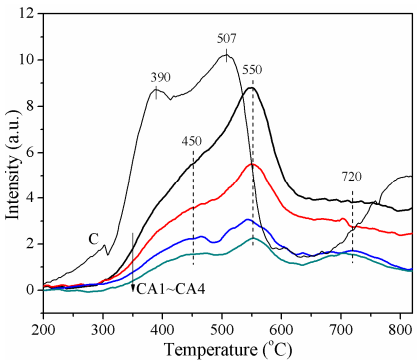

Fig. 2 H_2-TPR of CA composite, using C as a reference

On the other hand, the peak shift of the surface/subsurface oxygen indicates that the crystalline surface becomes more difficult to be reduced, as a result of CeO_2-Al_2O_3 interaction. But the peak of the bulk oxygen shifts to a reverse direction. According to literatures, Eleonora et al. [12] studied the H_2-TPR on CeO_2, and found a significant decrement of BET surface area at the beginning of the last reduction peak. So they concluded that the last peak, according to the bulk-like oxygen, is related with a re-construction of CeO_2 crystalline during the experiment. Therefore, the evolution of the last peak (weakened, and shifted to lower temperature) can be explained by that the reconstruction of CeO_2 crystalline is limited by the presence of Al_2O_3.

The microstructure of CA composite was detected under HR-TEM, using CA2-f as the example (Ce mole ratio 26 %). As shown in Fig. 3, the particle is in a spherical shape under TEM resolution. The un-uniformity of particle colour indicates the existence of CeO_2-rich and Al_2O_3-rich district. The edge of the particle in Fig. 5a was amplified step by step. And with the highest resolution (Fig. 5 D), the CeO_2 crystalline fringes can be identified (0.31 nm), attributed to CeO_2 (111) interplanar distance. However, no crystalline fringes can be identified on Al_2O_3, as a result of the poor crystallinity of alumina. In Fig. 3(D), several CeO_2 crystalline presented together, while another one is about several nanometre from them. Considering that the excess surface energy makes the crystalline aggregate spontaneously, the isolated presented CeO_2 indicates the existence of CeO_2–Al_2O_3 interaction which stabilizes the CeO_2 crystalline from its neighbours.

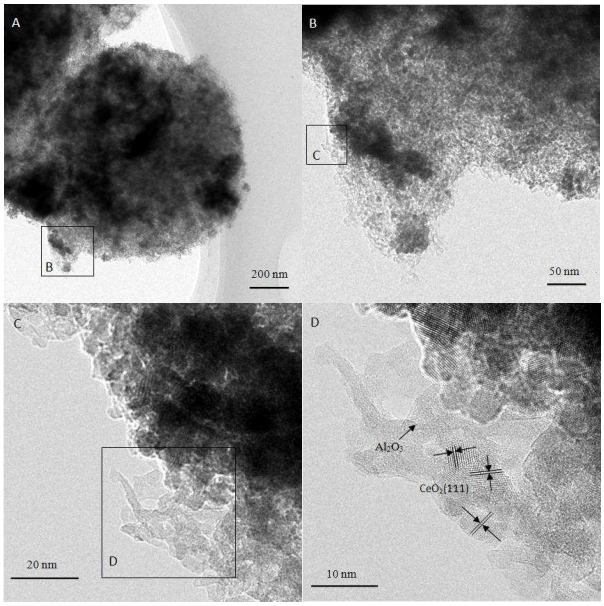

Fig. 3 Sample structure under (HR) TEM (CA2-f, B,C and D was the amplification of the cubic district in the former image.)

3.2 Evolution of microstructure in hydrothermal aging

The evolution of microstructure after aging is studied. As shown in Table 1, the surface area of CeO_2 (C) and Al_2O_3 (A) are 140 and 469 m^2/g, respectively, while the value of CA composite increases as the ratio of CeO_2 decreases. After 750 ˚C hydrothermal aging, the surface area of pure oxides decreases to 32 (CeO_2) and 240 m^2/g (Al_2O_3), and the value of CA sample is between 157 and 225 m^2/g, which increases as the CeO_2 ratio decreases. After 1050 ˚C aging, the surface area of pure oxide decreases to 3 (CeO_2) and 42 (Al_2O_3) m^2/g, respectively, but the value of CA is between 49 and 98 m^2/g. This indicates a superior hydrothermal stability of the CA composite comparing with the pure oxide.

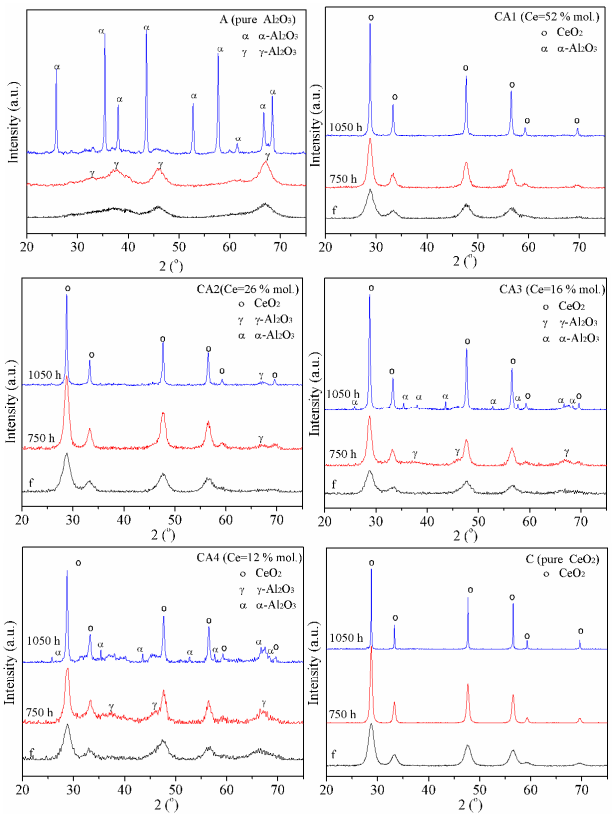

Fig. 4 XRD patterns of the samples before and after hydrothermal aging

XRD patterns are displayed in Fig. 2. On pure CeO_2, only cubic fluorite phase is observed, and the diffraction peaks of the aged sample are sharpened after aging, indicates the increment of CeO_2 crystalline size. On pure Al_2O_3, the main phase of fresh and 750h samples is γ-Al_2O_3, which changes to α-phase after 1050 ˚C aging. On CeO_2-Al_2O_3 composite, the main peaks of the fresh samples are cubic fluorite phase of CeO_2, even when the Ce mole ratio is 12 %. 750 ˚C hydrothermal aging does not induce obvious difference to the diffraction patterns, and CeO_2 crystalline size calculated by the peak width (2θ=28.6˚, (111)) shows limited growth comparing with the results of fresh samples (from 5 to 8 nm). Meanwhile, γ-Al_2O_3 was only observed on C3 and C4, as a wide shoulder at 2θ=46˚. This can be attributed to the low crystallinity of alumina, which is covered by the presence of CeO_2. After 1050 ˚C aging, the crystalline growth of CeO_2 becomes obvious, and a smaller Ce content induces a smaller crystalline size. Meanwhile, the relative intensity of α-Al_2O_3 becomes stronger (based on the one of Ce(111) diffraction peak) with the Ce content decreases. According to the above results, the decrement of surface area induced by 750 ˚C hydrothermal aging (from ~400 to ~200 m^2/g) can be attributed to either the phase transition (from amorphous to γ- phase) of Al_2O_3, or the crystalline growth of CeO_2. On the contrary, the further decrement of surface area in 1050 ˚C aging indicates a significant sintering, which is accompanied by the crystalline growth of CeO_2 and γ-α phase transition of Al_2O_3. It is noteworthy that the crystalline growth of CeO_2 is in reverse correlation with the formation of α-Al_2O_3, indicates that the sintering of the two oxides is independent with each other.

HR-TEM images after 1050 ˚C hydrothermal aging are collected on CA2 -1050h (as shown in Fig. 6). With TEM resolution (Fig. 5A), the edge of particle becomes more distinct, which indicates significant

enlargement of the crystalline. A particle fragment was found (should be obtained by ultrasonic treatment), which allows the investigation of the microstructure of CA composite. As shown in Fig. 6b, the crystalline presented in the image have two different shapes, the polygon and spherical crystalline. Phase attribution was identified by measuring the interplanar distance of the crystalline. In Fig. C and D, the interplanar distance is about 0.31 nm on the polygon crystalline, which is attributed to CeO_2 (111) face. In Fig. E, the interplanar distance of the spherical crystalline is 0.21 and 0.25 nm, which can be attributed to α-Al_2O_3 (113) and (104) face, respectively. The crystalline size of CeO_2 (polygon) agrees well with the result of XRD. However, the existence of α-Al_2O_3 in size of 5~10 nm indicates that γ-α phase transition occurs without sintering. In order to confirm the effect of CeO_2 to Al_2O_3 sintering, the particle of CA4-1050h is also investigated under HR-TEM (Fig. 6 F). Comparing with CA2-1050h, the well defined crystalline in size of about 500 nm can be attributed to the sintered α-Al_2O_3, and the result agrees well with XRD, that the Al_2O_3 sintering is more serious as Ce content decreases. Therefore, the sintering of CeO_2 and Al_2O_3 is independent with each other, and the presence of CeO_2 does not stop the γ-α phase transition, but hinders the sintering of α-Al_2O_3.

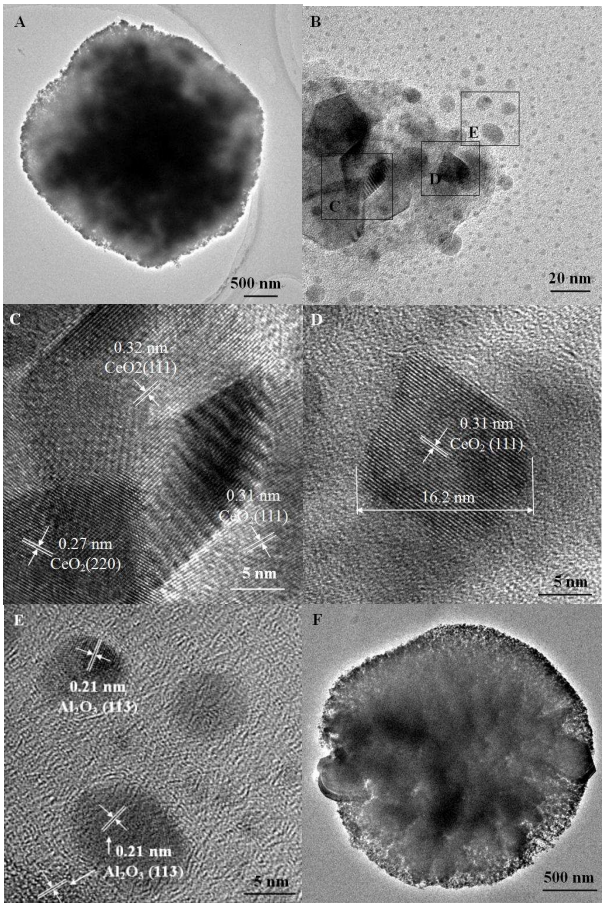

Fig. 5 (HR) TEM image of CA composite after 1050 ˚C aging. (A, a full particle of CA2; B~E, a fragment of CA2, C, D and E is the amplification of the cubic district in Fig. B. F, a particle of CA4-GH)

3.3 Dynamic Oxygen storage capacity (DOSC)

The DOSC calculated with 0.1 Hz frequency cycle was studied. On the fresh sample, the DOSC becomes smaller in the order of CA1>CA2>CA3>CA4, attributed to the CeO_2 content (50~10% in CA1~CA4, while Al_2O_3 is irreducible). The hydrothermal aging does not change this order, but reducing the difference among the samples. Considering that the CeO_2 content will not be changed by aging, the efficiency of CeO_2 clearly depends on the aging treatment, and may be influenced by CeO_2 content. So, the results were normalized by CeO_2 weight, as shown in Fig. 6. On the fresh samples, the specific DOSC (based on CeO_2 weight) decreases as the CeO_2 content decreases (including the pure CeO_2), indicates that CeO_2 surface becomes less active when the CeO_2 content is decreased. After 750 ˚C hydrothermal aging, the DOSC-temperature curve becomes independent of Ce content, indicates that the CeO_2 crystalline becomes similar on all the CA composites. Meanwhile, the specific DOSC of CA composite is much higher than the one of pure CeO_2, which is attributed to the superiority of the

hydrothermal stability (see XRD/BET results). After 1050 ˚C hydrothermal aging, the larger CeO_2 content induces lower specific DOSC, indicates that the sample with lower CeO_2 content suffers a smaller deactivation (comparing the results of 750h and 1050h). The results indicate that 750 ˚C hydrothermal aging improves the specific DOSC at low temperature (<500 ˚C), and makes it less sensitive to temperature. And the 1050 ˚C hydrothermal aging decreases the specific DOSC, while the decrement becomes limited as the CeO_2 content decreases.

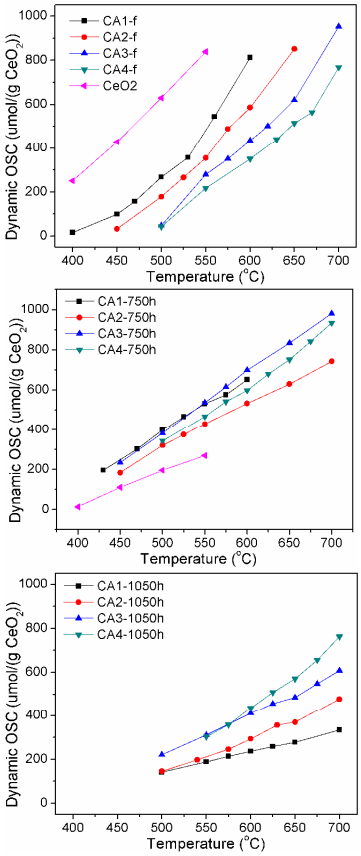

Fig. 6 Temperature dependence of DOSC (normalized by CeO_2 content)

For the evolution of DOSC agrees well with the sintering of CeO_2 crystalline, the oxygen storage capacity was calculated based on CeO_2 surface area. The CeO_2 surface area was calculated by the average crystalline size obtained in XRD (Table 1), using a spherical assumption as shown in the following equation:

$$S = \frac{S^*}{m} = \frac{S^*}{\rho V^*} = \frac{\pi D^2}{\rho \times 1/6\pi D^3} = 6/\rho D$$

where S and m are the surface area and weigh of the sample, respectively; S*, V* and ρ indicates the surface area, volume and density of CeO_2 crystalline, 7.1 g/cm^3. The results of pure CeO_2 (fresh and 750h) was displayed as references. As shown in Fig. 7, the specific DOSC decreases as the CeO_2 content decreases on the fresh samples, and increases as the sintering degree increases. Furthermore, comparing with the pure CeO_2, the specific DOSC per surface area of CA composites is lower than pure CeO_2, which increases to a similar value after 1050 ˚C hydrothermal aging. It indicates that the smaller CeO_2 content and more significant sintering (crystalline growth) benefits the specific OSC.

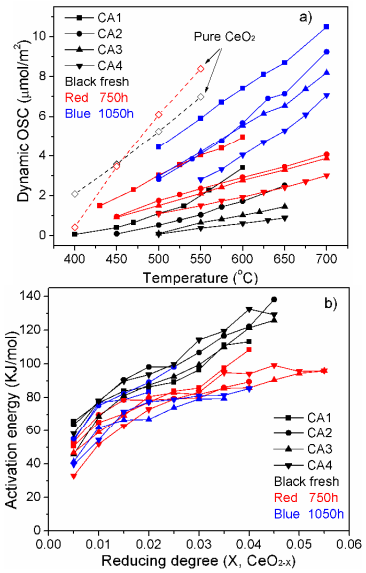

Fig. 7 The specific DOSC based on the CeO_2 surface area (a) and the activation energy as the function of reducing degree (b).

In order to further understand the evolution of DOSC, the activation energy is calculated as the function of reducing degree. The fundamental assumption of this calculation is that all the CeO_2 is effective [13, 14], and the details of the calculation are presented in supplementary materials. As displayed in Fig. 7 (bottom), the correlation between Ea and reducing degree only depends on the aging treatment, which is independent to CeO_2 content. On fresh samples, Ea increases monotonically as the reducing degree increases from ~60 to ~120 KJ/mol, indicates that the Oxygen release becomes more difficult as the sample is reduced. After 750 ˚C hydrothermal aging, Ea becomes smaller (increases from ~50 to ~100 KJ/mol), and Ea becomes independent to the reducing degree after a certain reduction.

In the oxygen storage materials, the oxygen release will become more difficult as more oxygen was released, which can be identified by an increased activation energy [14]. Furthermore, it and can be attributed to the more significant influence of oxygen transition from the bulk to the surface, which have a higher activation energy [15]. Therefore, a more sensitive Ea indicates that the transition of oxygen from the bulk is easier, and the insensitive part indicates that the oxygen transition is so easy, that the oxygen release is the limiting step. As shown in Fig. 7-b, and the sensitivity of Ea to the reducing degree (the slope in) becomes smaller after 750 ˚C and 1050 ˚C aging. It indicates that the supplementary of oxygen to the sample surface becomes easier in the aged samples. On the other hand, the 1050h samples show similar Ea~ reducing degree curves as those of 750h samples. Therefore, the sintering does not hinder the supplementary of surface oxygen, but reduces the total amount of oxygen release rate as a result of sintering of CeO_2.

3.4 CeO_2-Al_2O_3 interaction

The combination of support material (strong interaction with the active component but low stability) and wall material (stronger stability) in nano scale has been applied to improve the stability of the catalysts [16, 17]. However, the possible interaction between the two materials is speculated, which can be further understood by combining the results of structural and DOSC studies.

The evolution between fresh and 750h samples indicates a strong interaction between CeO_2 and Al_2O_3. The interaction between CeO_2 and Al_2O_3 was identified by the uniform chemical circumstance of CeO_2 (H_2-TPR) and the stuck of CeO_2 crystalline on Al_2O_3 framework (HR-TEM). On the other hand, 750 ˚C hydrothermal aging does not induce significant increment of CeO_2 crystalline size, but the Ea of DOSC becomes insensitive to the reducing degree after a certain reduction. Considering that 750 ˚C is only high enough to CeO_2 sintering (not to the Al_2O_3), the evolution of 750 ˚C aging is attributed to a reconstruction of CeO_2 with the restriction of Al_2O_3 framework. Therefore, the strong interaction between CeO_2 and Al_2O_3 has a negative effect on the DOSC of the sample, but it can be easily eliminated.

On the other hand, the results of two different aged samples indicate that the reason of improved hydrothermal stability is attributed to the spatial limitation, while chemical interactions should not be included. 750 ˚C hydrothermal aging only allows the sintering of CeO_2, and 1050 ˚C aging allows the sintering of both CeO_2 and Al_2O_3. Although the 1050 ˚C hydrothermal aging induces more serious sintering, the correlation between Ea and reducing degree is similar to the results of 750h. Therefore, the improvement of hydrothermal stability cannot be attributed to the chemical interaction, for the interaction only exists on fresh sample. Considering that the sintering of the two components is

independent, the good hydrothermal stability is attributed to the spatial limitation.

4. Conclusions

CeO_2-Al_2O_3 composite was prepared by a two step protocol, including the separate preparation of CeO_2 crystalline dispersion and Al_2O_3 sol, and a quick drying process of the mixture using spraying drying method. The sample resists about 79~90 m^2/g BET surface area even after 1050 ˚C 10 h hydrothermal aging, which is good enough for the application of exhaust aftertreatment. Based on the characterizations and DOSC test, the interaction between CeO_2 and Al_2O_3 is separated into two parts: 1) CeO_2-Al_2O_3 interaction which decreases the specific activity of DOSC, and 2) a spatial limitation which benefits the hydrothermal stability. The first one can be eliminated by a 750 ˚C 20 h aging.

Acknowledgements

The work was financially supported by the introduction of talent and technology cooperation plan of Tianjin (14RCGFGX00849).

Supplementary materials

S1. Details of the dynamic oxygen storage capacity calculation

References

1 C.W. Sun, H. Li, L.Q. Chen, *Energy Environ. Sci.* 2012, **5**, 8475.

2 W.S. Epling, L.E. Campbell, A. Yezerets, N.W. Currier, J.E. Parks, *Catal. Rev.-Sci. Eng.* 2004, **46**, 163.

3 M. Cargnello, V.V.T. Doan-Nguyen, T.R. Gordon, R.E. Diaz, E.A. Stach, R.J. Gorte, P. Fornasiero, C.B. Murray, *Science* 2013, **341**, 771.

4 S.K. Matam, E.V. Kondratenko, M.H. Aguirre, P. Hug, D. Rentsch, A. Winkler, A. Weidenkaff, D. Ferri, *Appl. Catal. B, Environ.* 2013, **129**, 214.

5 C. Tyrsted, K.M.Ø. Jensen, E.D. Bøjesen, N. Lock, M. Christensen, S.J.L. Billinge, B.B. Iversen, *Angew. Chem. Int. Ed.* 2012, **51**, 9030.

6 H.R. Chen, Z.Q. Ye, X.Z. Cui, J.L. Shi, D.S. Yan, *Microporous Mesoporous Mater.* 2011, **143**, 368.

7 Q.Y. Wang, Z.G. Li, B. Zhao, G.F. Li, R.X. Zhou, *J. Mol. Catal. A: Chem.* 2011, 344, 132.

8 K.M.S. Khalil, *J. Colloid Interface Sci.* 2007, **307**, 172.

9 T.A. Maia, J.M. Assaf, E.M. Assaf, *Fuel Prosess. Technol.* 2014, **128**, 134.

10 M.H. Jiang, B.W. Wang, Y.Q. Yao, Z.H. Li, X.B. Ma, S.D. Qin, Q. Sun, *Appl. Surf. Sci.* 2013, **285P**, 267.

11 H.-J. Sédjame, C. Fontaine, G. Lafaye, J. B. Jr, *Appl. Catal. B Environ.* 2014, **144**, 233.

12 E. Aneggi, A. Trovarelli, C. de Leitenburg, G. Dolcetti, A. Trovarelli, *J. Alloys Compounds*, 2006, **408-412**, 1096.

13 C.E. Hori, A. Brenner, K.Y. Simon Ng, K.M. Rahmoeller, D. Belton, *Catal. Today* 1999, **50**, 299.

14 M. Yang, M.Q. Shen, J. Wang, J. Wen, M.W. Zhao, J. Wang, W.L. Wang, *J. Phys. Chem. C*, 2009, **113**, 12778.

15 M. Zhao, M. Shen, J. Wang, *J. Catal.* 2007, **248**, 258.

16 M. Nakamura, H. Wakamatsu, K. Suga, T. Sekiba, Y. Hiramoto, K. Shibata, *SAE Int.* 2009-01-1069.

17 Y. Aoki, S. Sakagami, M. Kawai, N. Takahashi, T. Tanabe, T. Sunada, *SAE Int.* 2011-01-0296.